PHYSICAL REVIEW LETTERS **133,** 056701 (2024)

Editors' Suggestion

Separation of Inverse Altermagnetic Spin-Splitting Effect from Inverse Spin Hall Effect in RuO_2

Ching-Te Liao,[1] Yu-Chun Wang,[1] Yu-Cheng Tien,[1] Ssu-Yen Huang,[1,2,*] and Danru Qu[2,3,†]
[1]*Department of Physics, National Taiwan University, Taipei 10617, Taiwan*
[2]*Center of Atomic Initiatives for New Materials, National Taiwan University, Taipei 10617, Taiwan*
[3]*Center for Condensed Matter Sciences, National Taiwan University, Taipei 10617, Taiwan*

(Received 29 February 2024; accepted 20 June 2024; published 30 July 2024)

Presented by: Kaushal K. Kesharpu
At: BLTP Journal club
On: 16/09/2024

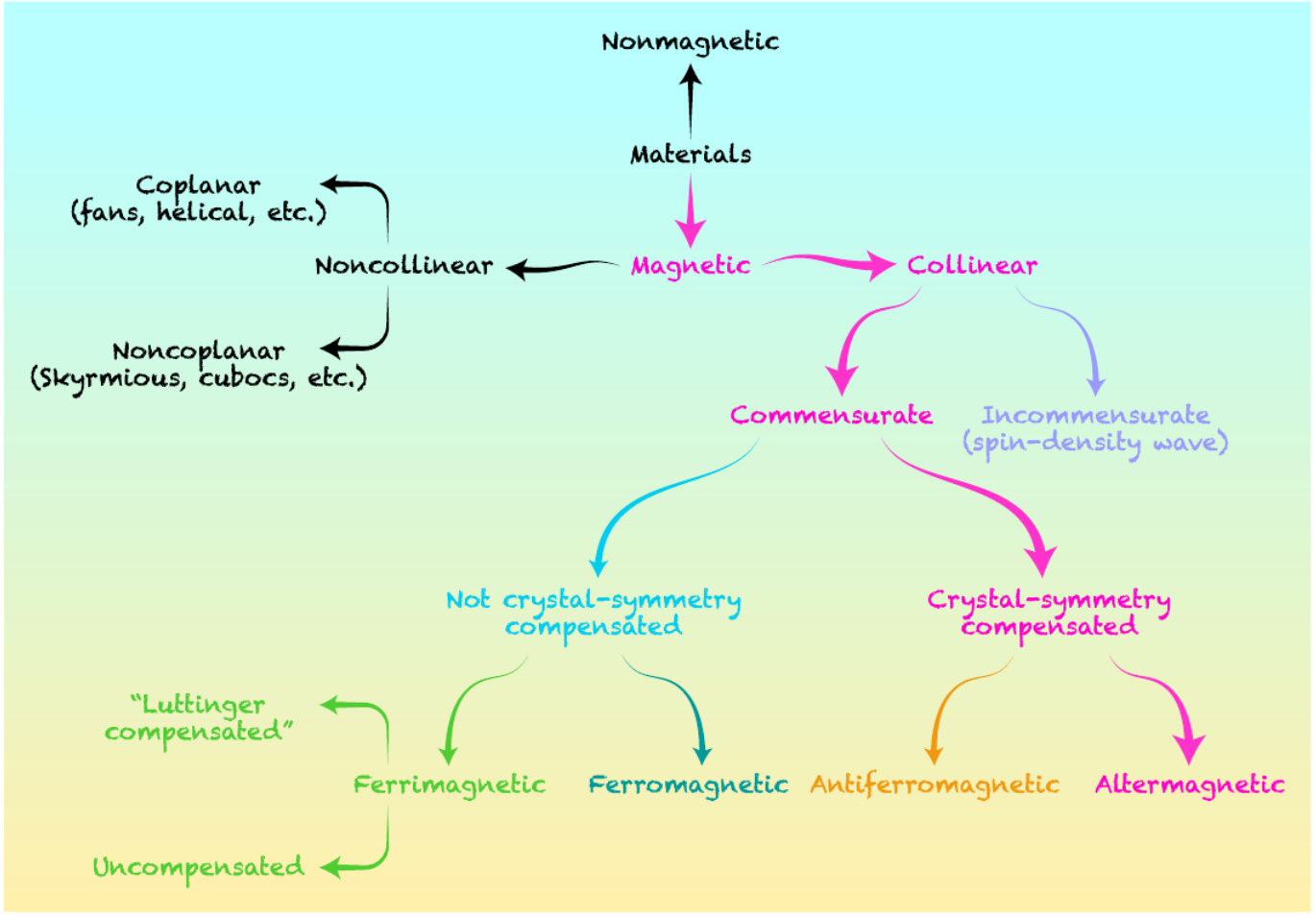

FIG. 1. A comprehensive classification scheme of different magnetic orders that shows altermagnetism as a fundamentally new class of magnetic order.

Igor Mazin and The PRX Editors Phys. Rev. X 12, 040002

PHYSICAL REVIEW X **12,** 040501 (2022)

Emerging Research Landscape of Altermagnetism

Libor Šmejkal,[1,2] Jairo Sinova,[1,2] and Tomas Jungwirth[2,3]

[1]*Institut für Physik, Johannes Gutenberg Universität Mainz, D-55099 Mainz, Germany*
[2]*Institute of Physics, Czech Academy of Sciences, Cukrovarnická 10, 162 00 Praha 6 Czech Republic*
[3]*School of Physics and Astronomy, University of Nottingham, Nottingham NG7 2RD, United Kingdom*

(Received 15 March 2022; revised 15 August 2022; published 8 December 2022)

Magnetism is one of the largest, most fundamental, and technologically most relevant fields of condensed-matter physics. Traditionally, two basic magnetic phases have been distinguished ferromagnetism and antiferromagnetism. The spin polarization in the electronic band structure reflecting the magnetization in ferromagnetic crystals underpins the broad range of time-reversal symmetry-breaking responses in this extensively explored and exploited type of magnets. By comparison, antiferromagnets have vanishing net magnetization. Recently, there have been observations of materials in which strong time-reversal symmetry-breaking responses and spin-polarization phenomena, typical of ferromagnets, are accompanied by antiparallel magnetic crystal order with vanishing net magnetization, typical of antiferromagnets. A classification and description based on spin-symmetry principles offers a resolution of this apparent contradiction by establishing a third distinct magnetic phase, dubbed altermagnetism. Our perspective starts with an overview of the still emerging unique phenomenology of this unconventional *d*-wave (or higher even-parity wave) magnetic phase, and of the wide array of altermagnetic material candidates. We illustrate how altermagnetism can enrich our understanding of overarching condensed-matter physics concepts and how it can have impact on prominent condensed-matter research areas.

DOI: 10.1103/PhysRevX.12.040501

Subject Areas: Condensed Matter Physics
Magnetism, Spintronics

L. Smejkal

J. Sinova

Materials which show partially the properties of both AFM and FM are called the Altermagnetic materials.

TABLE I. A comparative summary of the phenomenological similarities and differences between altermagnets and the familiar ferromagnets as well as antiferromagnets.

	FM	AF	AM
Nonrelativistic net magnetization	nonzero or zero	zero	zero
Nonrelativistic Kramers spin degeneracy	no	yes	no
Anomalous Hall	yes	no	yes
Magnetooptics	yes	no	yes
Nonrelativistic spin-polarized current	yes	no	yes
Suppression of Andreev reflection: diffuse contact	yes	no	no
Suppression of Andreev reflection: ballistic contact	yes	no	yes
Supports singlet superconductivity	no	yes	no
Supports locally (in k-space) unitary triplet superconductivity	no	yes	no
Supports k-averaged unitary triplet superconductivity	no	yes	yes
Giant or tunneling magnetoresistance and spin-transfer torque	yes	no	yes

Igor Mazin and The PRX Editors Phys. Rev. X 12, 040002

Table 1 | **List of experimentally identified anomalous Hall antiferromagnets**

Order	System	Synthesis	T_N (K)	ρ_H ($\mu\Omega$ cm)	σ_{AH} (S cm^{-1})	T (K)	H (T)	Space group and MSG	Other systems
NC	Mn_3Sn (REF.[22])	SC	420	4	20	300	0	$P6_3/mmc$ and $Cm'cm'$	–
	Mn_3Ge (REFS[23,24])	SC	380	0.1	400	5	0.1	$P6_3/mmc$ and $C2'/m'$	–
	Mn_3Pt (REF.[105])	20 nm	360	–	98	20	0	$Pm\bar{3}m$ and $R\bar{3}m'$	–
	Mn_3Sn (REF.[123])	40 nm	>300	1.5	17	300	0	$P6_3/mmc$	–
	*Mn_3Sn (REF.[124])	30 nm epitaxial	–	0.05	21	300	0	$P6_3/mmc$	–
C	RuO_2 (REF.[42])	27 nm	>300	0.05	330	10	30	$P4_2/mnm$ and $Pnn'm'$	–
	Mn_5Si_3 (REF.[43])	12 nm epitaxial	240	0.3	5	110	0	$P6_3/mcm$ and $\bar{1}$	–
	(Ca,Ce)MnO_3 (REF.[172])	20 nm	~120	1	–	15	1–1.5	$Pnma$ and $Pn'ma'$	–
	*$CoNb_3S_6$ (REF.[160])	SC	27.5	1	27	23	0	$P6_322$	–
	*$CoNb_3S_6$ (REF.[173])	40–90 nm	29	2	400	5	0	$P6_322$	–
NCP	*$Pr_2Ir_2O_7$ (REFS[19,174])	SC	~20	1	10	1	0	$Fd\bar{3}m$	UCu_5 (REF.[75]), $Nd_2Ir_2O_7$ (REF.[175])
	Mn_5Si_3 (REFS[76,159,176])	SC, 40–160 nm	66	2	102	25	5	$P6_3/mcm$ and $PCbcn$	–
CA	GdPtBi (REF.[177])	SC	9.2	60	30–200	10	4	$F\bar{4}3m$ and C_cc	Gd(Nd)PtBi (REF.[178])
	$EuTiO_3$ (REF.[179])	SC	5.5	5	20	2	2	$I4/mcm$ and $Fm'mm$	Eu(Sm)TiO_3 (REF.[180]), $Nd_2Ir_2O_7$ (REF.[181])

We group the materials into four archetypes: non-collinear coplanar (NC), collinear (C), non-coplanar (NCP) and canted (CA). We also list whether the material was synthesized as a bulk single crystal (SC) or as a thin film (of a given thickness). Next, we list the Néel temperature ($\mathcal{T}_N$), Hall resistivity (ρ_H) and conductivity (σ_{AH}), the temperature of the experiments ($\mathcal{T}$) and the applied magnetic field (H). Finally, we list the crystal space group and magnetic space group (MSG), and other systems with corresponding structure in which Hall measurements were also reported. Asterisks mark systems with unconfirmed magnetic ordering.

Šmejkal, L., MacDonald, A.H., Sinova, J. et al. Anomalous Hall antiferromagnets. Nat Rev Mater 7, 482–496 (2022).

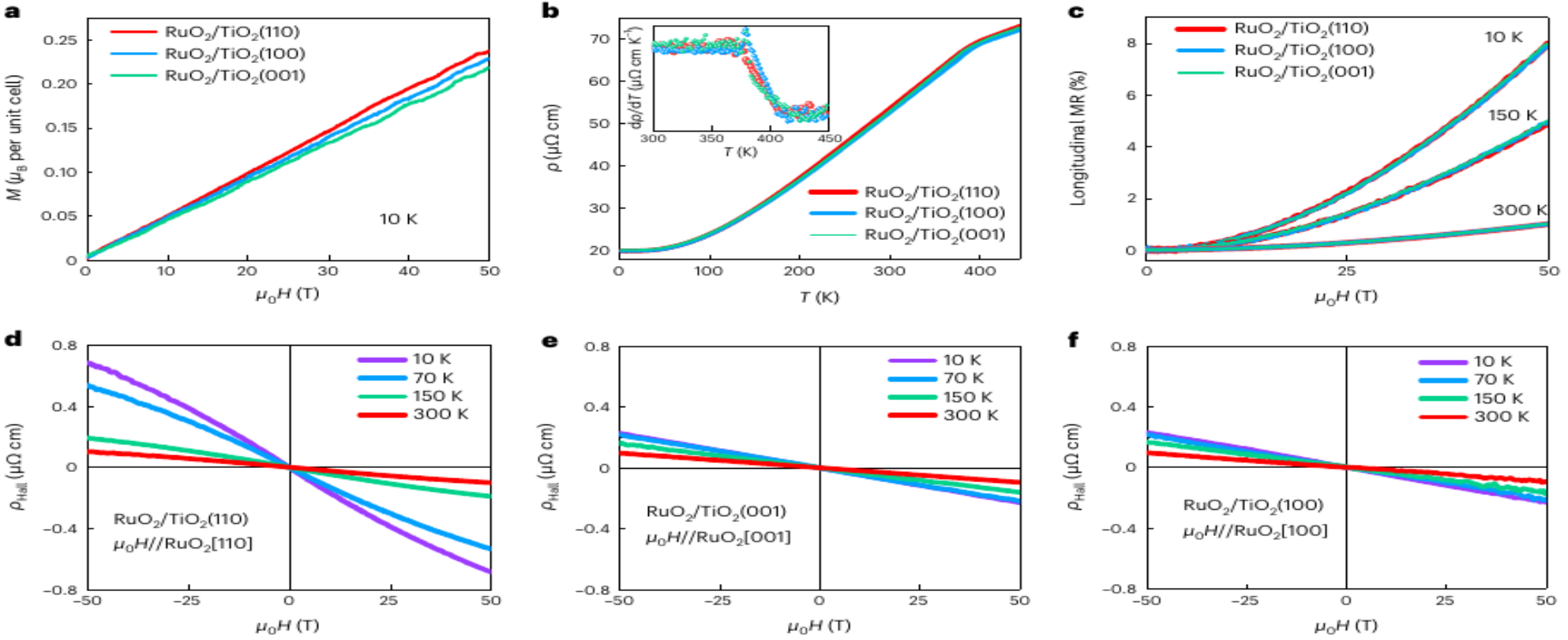

Fig. 2 | Magnetization and magneto-transport measurements. **a**, Magnetization M along the applied out-of-plane magnetic field $\mu_0 H$ for the three RuO_2/TiO_2 film orientations. **b**, Resistivity ρ versus temperature T for the three film orientations. The inset shows the temperature derivative of resistivity, highlighting the Néel-temperature transport anomaly. **c**, Longitudinal magnetoresistance (MR) in the applied out-of-plane magnetic field at different temperatures. **d**–**f**, Hall resistivity ρ_H at different temperatures for the three film orientations of (110) (**d**), (001) (**e**) and (100) (**f**).

Feng, Z., Zhou, X., Šmejkal, L. et al. An anomalous Hall effect in altermagnetic ruthenium dioxide. Nat Electron 5, 735–743 (2022).

Magnetism's new twist

The properties of most magnetic materials depend on whether each atom's magnetic field—denoted by its spin—is pointing up (pink) or down (blue). In altermagnets, the atoms and their spins rotate independently, giving them properties of both ferromagnets and antiferromagnets.

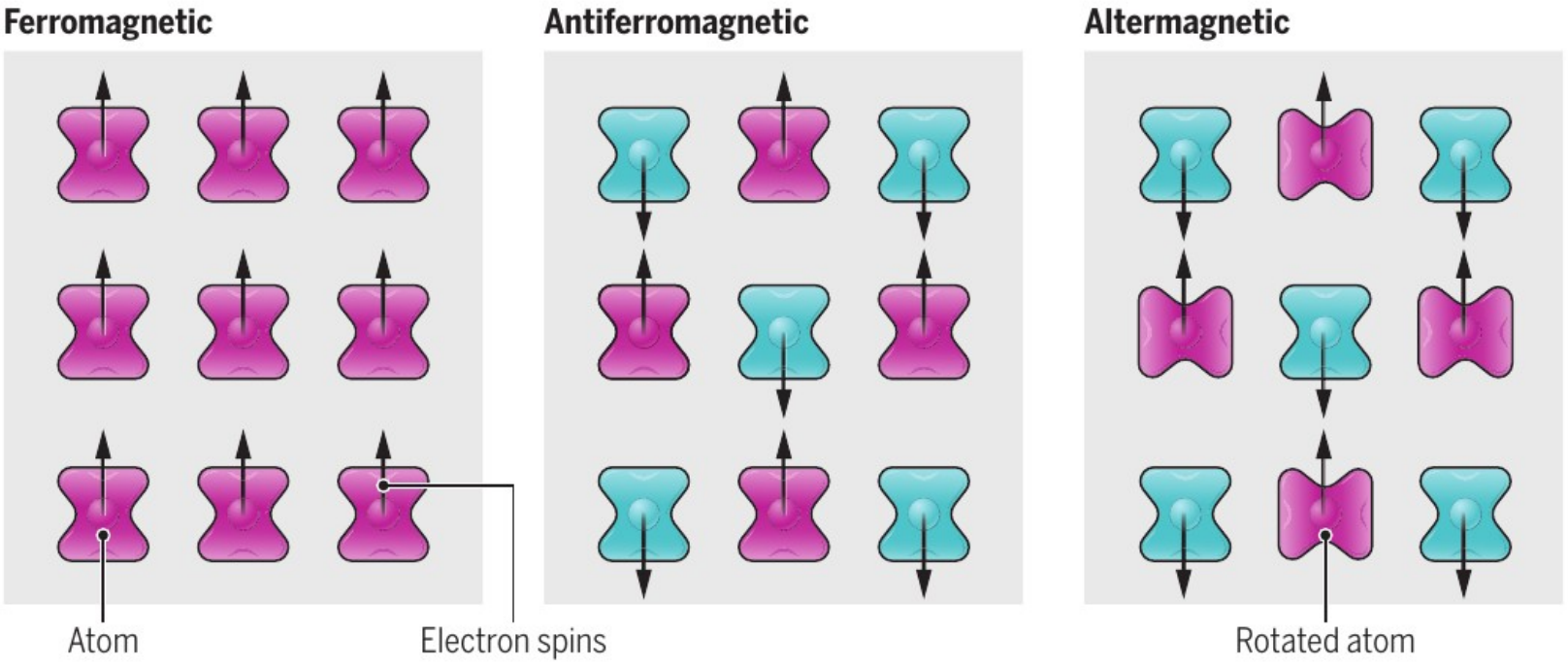

https://www.science.org/content/article/researchers-discover-new-kind-magnetism

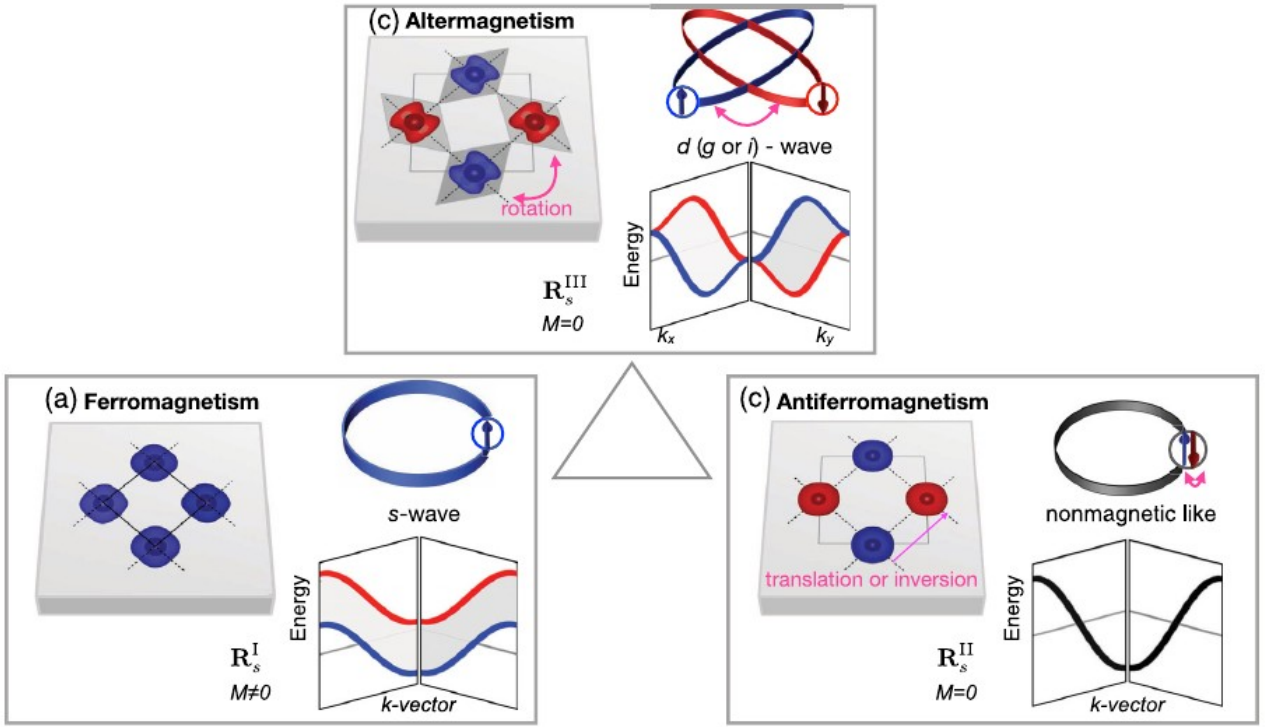

FIG. 1. Illustrative models of collinear ferromagnetism, antiferromagnetism, and altermagnetism in crystal-structure real space and nonrelativistic electronic-structure momentum space. (a) Ferromagnetic model with one spin sublattice, and corresponding distinct spin-group form, nonzero magnetization, $\mathcal{T}$-symmetry breaking momentum-independent spin splitting of bands, and isotropic s-wave spin-split Fermi surfaces. (b) Antiferromagnetic model with opposite-spin sublattices (red, blue) connected by inversion or translation, and corresponding distinct spin-group form, zero net magnetization, and $\mathcal{T}$-invariant spin-degenerate bands reminiscent of nonmagnetic systems. (c) Altermagnetic model with opposite-spin sublattices connected by rotation and not by translation or inversion, and corresponding distinct spin-group form, zero net magnetization, $\mathcal{T}$-symmetry breaking spin splitting with alternating sign, anisotropic sublattice spin densities, and anisotropic d (g or i)-wave spin-split Fermi surfaces. See Sec. II B for the definitions of the distinct spin-group forms $\mathbf{R}_s^i$.

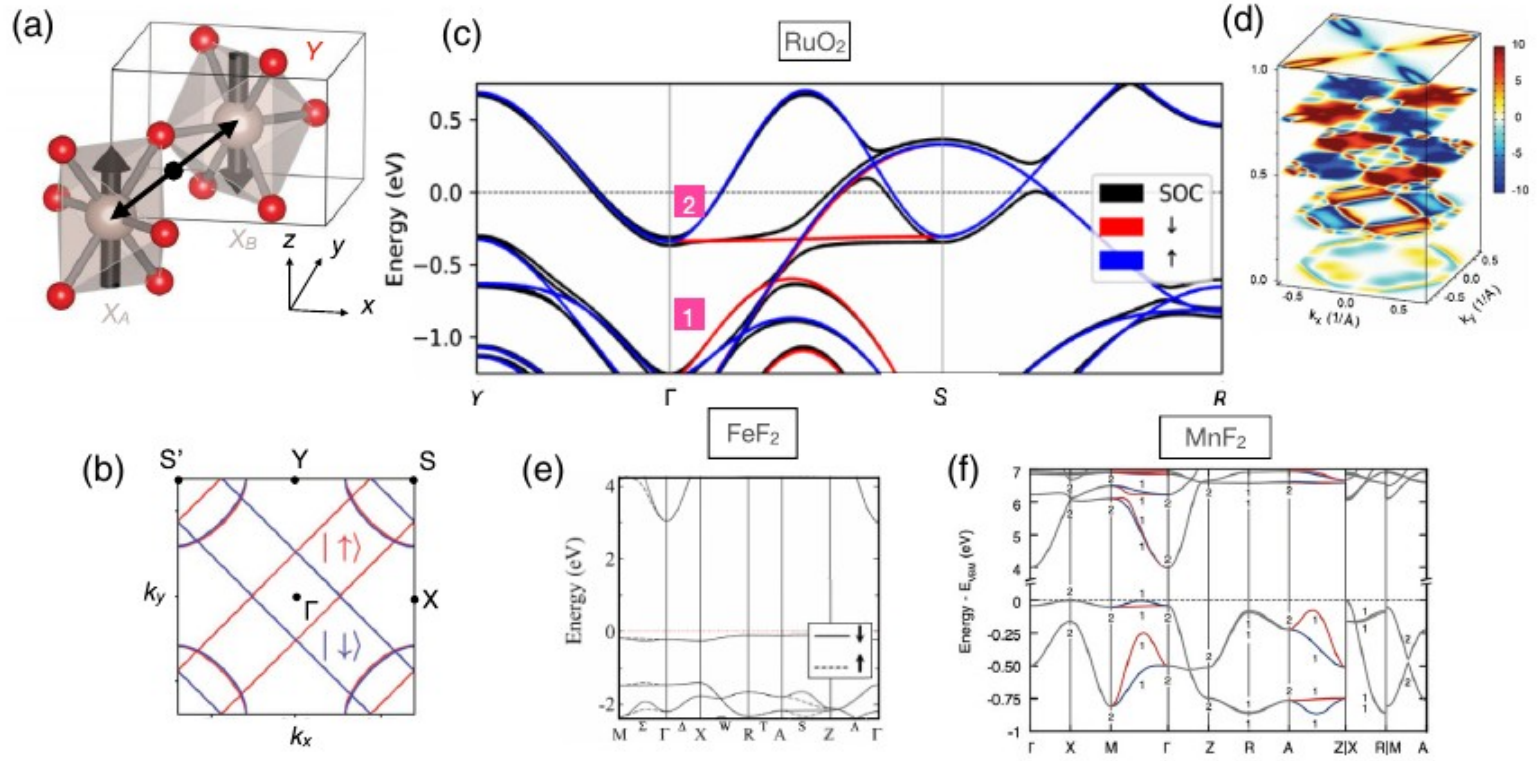

FIG. 3. (a) Schematics of the rutile XY_2 crystal structure with antiparallel magnetic moments on X_A and X_B magnetic sublattices. (b) Brillouin zone of the rutile crystal and *ab initio* nonrelativistic calculation of a wave-vector $k_z = 0$ cut of the anisotropic *d*-wave spin-polarized Fermi surface of metallic RuO_2. (c) *Ab initio* altermagnetic spin splitting of bands in RuO_2, calculated without (red and blue) and with (black) relativistic spin-orbit coupling. (d) *Ab initio* altermagnetic spin-split Fermi surface for selected k_z values in RuO_2 with correlations accounted for within the dynamical mean-field theory. (d,e) *Ab initio* altermagnetic spin-split bands of insulating FeF_2 and MnF_2, respectively. This figure is adapted from Refs. [3,18,20,47].

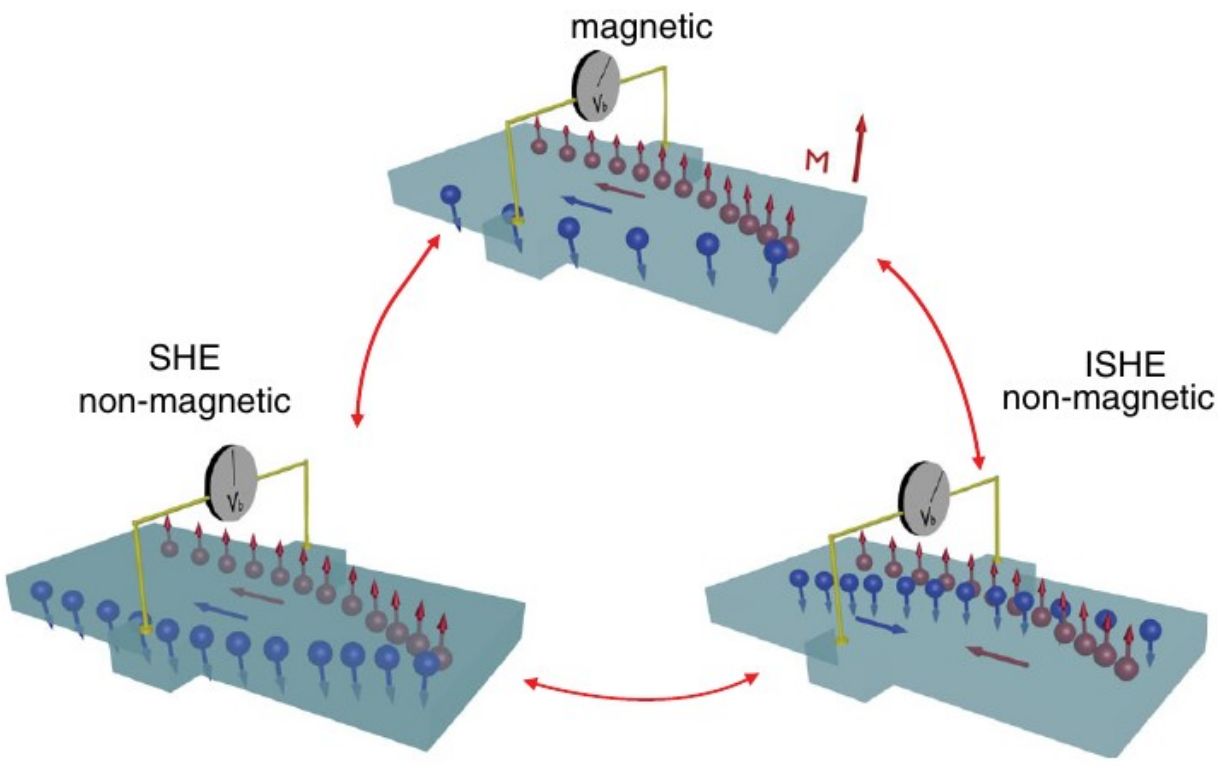

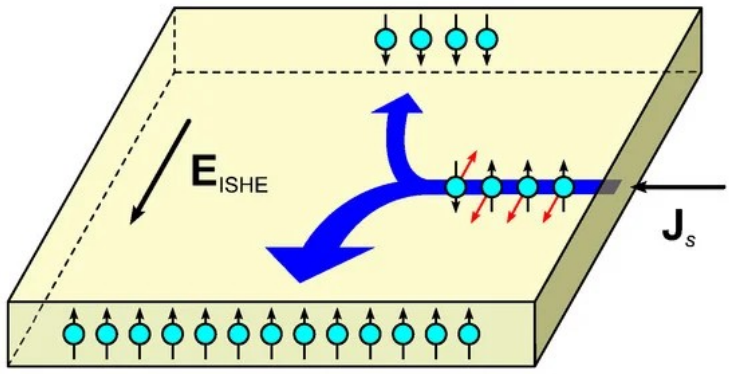

FIG. 1 (color online). An illustration of the connected family of the spin-dependent Hall effects. In the AHE, a charge current generates a polarized transverse charge current. In the SHE, an unpolarized charge current generates a transverse pure spin current. In the ISHE, a pure spin current generates a transverse charge current.

Jairo Sinova, Sergio O. Valenzuela, J. Wunderlich, C. H. Back, and T. Jungwirth

Rev. Mod. Phys. 87, 1213

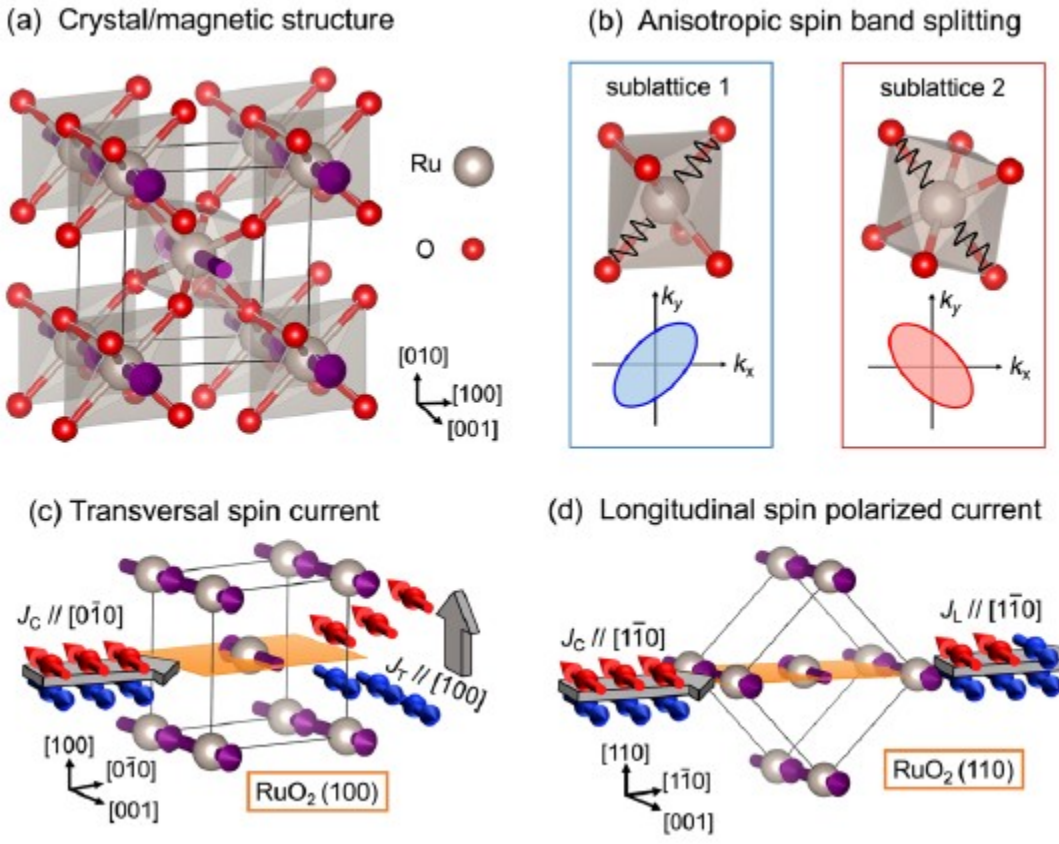

FIG. 1. (a) Crystal and magnetic structure of the rutile RuO_2. Gray and red spheres represent Ru and O atoms, respectively. Purple arrows mark the Ru local moments. (b) Schematic of the anisotropic spin band splitting in RuO_2. Oxygen octahedrons of two sublattices are rotated by 90°. The Ru atoms of two magnetic sublattices feel anisotropic octahedral crystal field (wavy black lines), leading to the anisotropic spin band splitting, as displayed by blue and red ellipses. (c) For the (100)-oriented RuO_2 film, transversal spin current (J_T) flowing along the [100] axis (out-of-plane) can be induced by the charge current along the $[0\bar{1}0]$ axis. The spin polarization is parallel to the Néel vector ([001] axis). (d) For the (110)-oriented RuO_2 film, spin polarized current (J_L) flowing along longitudinal direction can be generated by the charge current along the $[1\bar{1}0]$ axis. The spin polarization is also parallel to the Néel vector.

H. Bai, et. al. Phys. Rev. Lett. 128, 197202

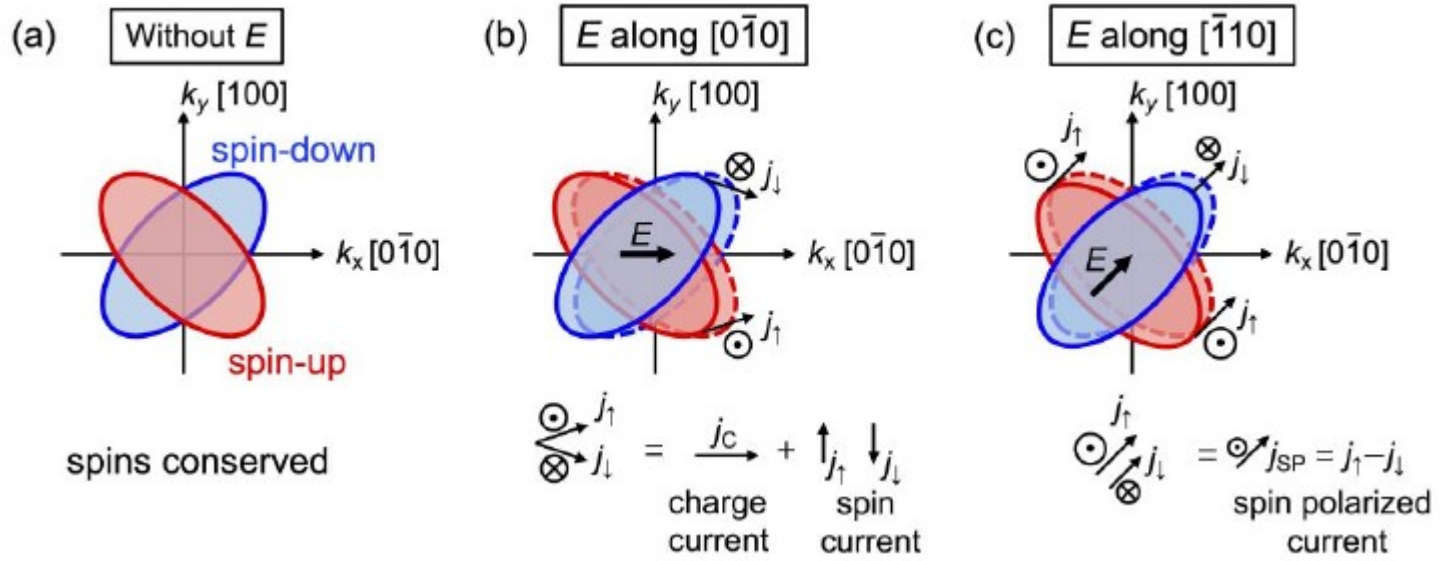

FIG. S1. Schematic of spin current generation induced by the shift of Fermi surface and the resultant anisotropic spin splitting effect (ASSE). (a) Anisotropic spin band splitting due to the 90° rotation of oxygen octahedrons in two magnetic sublattices. Red and blue ellipses represent the spin-up and spin-down bands, respectively. Without current/electric field applied, the macroscopic spin flowing is absent. (b) When the current/electric field is applied along [0$\bar{1}$0], the spin-up and spin-down bands are shifted along the same direction, giving rise to a charge current flowing along [0$\bar{1}$0] and a spin current flowing along [100]. (c) When the current/electric field is applied along [1$\bar{1}$0], spin bands are shifted along the same direction, giving rise to a spin polarized current flowing along [1$\bar{1}$0]. Here, ⊙ and ⊗ respectively represent spin-up and spin-down, and the diameters of circles denote the amount.

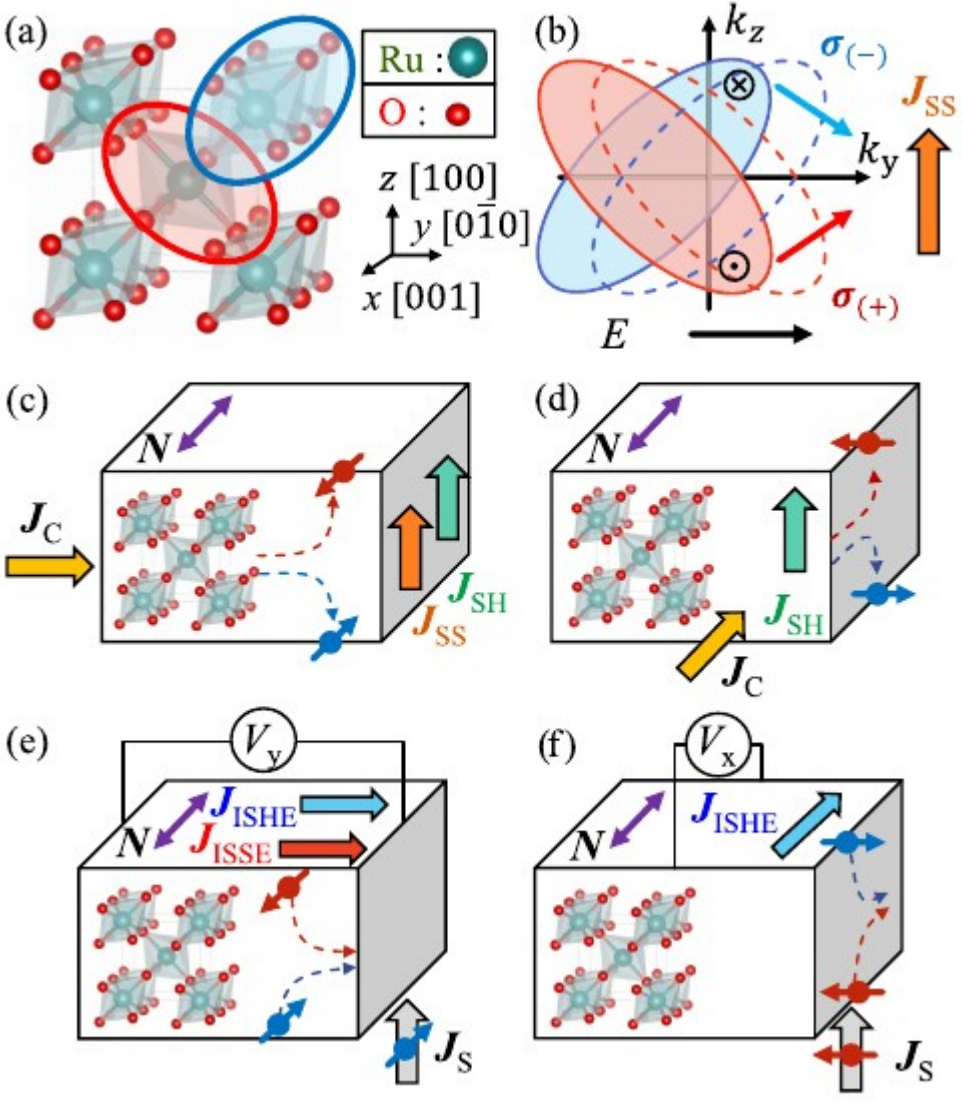

FIG. 1. Schematics of (a) the crystal structure and (b) the spin-splitting band of rutile RuO_2. When an electric field (E) is applied along the y axis, a spin-splitting current (J_{SS}) is generated in the transverse z axis by the nonrelativistic spin-splitting effect, which carries only angular momentum and no net charge. Schematics of the (c) presence and (d) absence of J_{SS} caused by the direction of the incident charge current (J_C) perpendicular and parallel to the Néel vector (N), respectively. Schematics of the (e) presence and (f) absence of the inverse spin-splitting current (J_{ISSE}) caused by the direction of the spin index (σ) of the incident spin current (J_S) parallel and perpendicular to N, respectively.

Ching-Te Liao et. al. Phys. Rev. Lett. 133, 056701

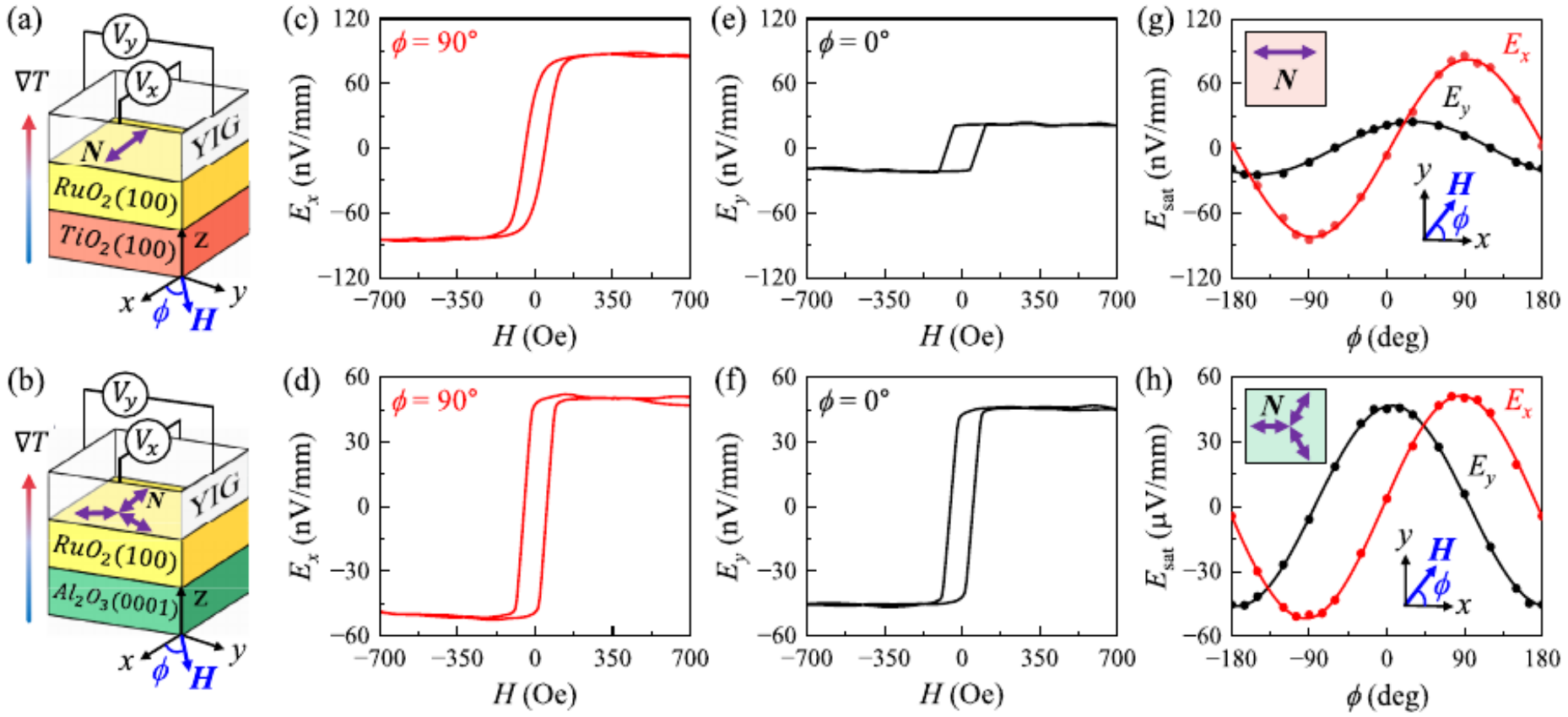

FIG. 3. Schematics of experiment setups of (a) YIG/RuO_2/TiO_2 and (b) YIG/RuO_2/Al_2O_3 samples. The x axis is set along the [001] direction of TiO_2 and along the $[01\bar{1}0]$ direction of Al_2O_3. φ is the angle between the external magnetic field and the x axis. The *spin-to-charge* conversion electric field is measured along the (c) x and (e) y axes of YIG/RuO_2 on TiO_2, and along the (d) x and (f) y axes of YIG/RuO_2 on Al_2O_3. φ-dependent *spin-to-charge* conversion electric field for YIG/RuO_2 on (g) TiO_2 and (h) Al_2O_3 substrates.